Evaluated Crop Evapotranspiration over a Region of Irrigated Orchards with the Improved ACASA–WRF Model

Evaluated Crop Evapotranspiration over a Region of Irrigated Orchards with the Improved ACASA–WRF Model

MATTHIAS FALK, R. D. PYLES, S. L. USTIN, AND K. T. PAW U

Department of Land, Air and Water Resources, University of California, Davis, Davis, California

L. XU

Department of Land, Air and Water Resources, University of California, Davis, Davis, California, and Center for Global Change Science, Massachusetts Institute of Technology, Cambridge, Massachusetts

M. L. WHITING

Department of Land, Air and Water Resources, University of California, Davis, Davis, California

B. L. SANDEN

University of California Cooperative Extension, Bakersfield, California

P. H. BROWN

Department of Plant Sciences, University of California, Davis, Davis, California

(Manuscript received 3 December 2012, in final form 15 November 2013)

ABSTRACT

Among the uncertain consequences of climate change on agriculture are changes in timing and quantity of precipitation together with predicted higher temperatures and changes in length of growing season. The understanding of how these uncertainties will affect water use in semiarid irrigated agricultural regions depends on accurate simulations of the terrestrial water cycle and, especially, evapotranspiration. The authors test the hypothesis that the vertical canopy structure, coupled with horizontal variation in this vertical structure, which is associated with ecosystem type, has a strong impact on landscape evapotranspiration. The practical result of this hypothesis, if true, is validation that coupling the Advanced Canopy–Atmosphere–Soil Algorithm (ACASA) and the Weather Research and Forecasting (WRF) models provides a method for increased accuracy of regional evapotranspiration estimates.

ACASA–WRF was used to simulate regional evapotranspiration from irrigated almond orchards over an entire growing season. The ACASA model handles all surface and vegetation interactions within WRF. ACASA is a multilayer soil–vegetation–atmosphere transfer model that calculates energy fluxes, including evapotranspiration, within the atmospheric surface layer.

The model output was evaluated against independent evapotranspiration estimates based on eddy covariance. Results indicate the model accurately predicts evapotranspiration at the tower site while producing consistent regional maps of evapotranspiration (900–1100 mm) over a large area (1600 km^2) at high spatial resolution ($\Delta x = 0.5$ km).

Modeled results were within observational uncertainties for hourly, daily, and seasonal estimates. These results further show the robustness of ACASA's ability to simulate surface exchange processes accurately in a complex numerical atmospheric forecast model such as WRF.

1. Introduction

Accurate spatial estimates of water use in irrigated orchards are crucial in California, where agriculture relies on irrigation water, either from groundwater

Corresponding author address: Matthias Falk, LAWR, Plant and Environmental Sciences Bldg., University of California, Davis, 1 Shields Ave., Davis, CA 95616.
E-mail: mfalk@ucdavis.edu

DOI: 10.1175/JHM-D-12-0183.1

sources or via surface water supplies. Agriculture is the largest water consumer in the state, consuming as much as 75% of the water supply in the mid-1990s (Vaux 1999). There are strong correlations between water availability and agricultural productivity and significant penalties for underirrigation. The combination of projected climate change for California and long-term competition for water resources, for example, from population growth, other industries, and demand from natural ecosystems, could lead to large overall reductions of water available to agricultural producers (Kiparsky and Gleick 2003).

Among the uncertain consequences of climate change on agriculture are changes in timing and quantity of precipitation, including less predictable and more variable interannual rainfall (Downing and Parry 1994; Houghton et al. 2001). On average, increasing CO_2 concentrations have been shown to improve C_3 crop net primary production (NPP) by 33% for a doubling of atmospheric CO_2 (Koch and Mooney 1996). Grassland and crop studies combined show an average biomass increase of 14%, with a wide range of responses among individual studies (Mooney et al. 1999). Field experiments suggest a more complex picture, with C_4 plants sometimes doing better than C_3 under elevated CO_2 because of improved water use efficiency at the ecosystem level (Owensby et al. 1993). Thus, other climate-related changes can outweigh the improved productivity due to increasing CO_2, particularly moving further into the future climate. Changes in water availability, combined with predicted higher temperatures and changes in length of growing season, will adversely impact food security. Water shortages are already common in semiarid regions, and climate predictions indicate increased frequency and intensity of droughts, leading to concerns about future security of food production. About 40% of the global land surface is considered semiarid, experiencing 500–1000 mm of precipitation annually and with at least one dry month, which is present on all continents except Antarctica. One-sixth of the world's population (~1.2 billion people) lives in and relies on food resources from these environments. These transition ecosystems experience exceedingly variable patterns of rainfall, often in just a few large storms, where water is lost to runoff and high rates of evapotranspiration (ET). Despite its semiarid Mediterranean climate and highly variable interannual winter-dominated precipitation, California is the largest agricultural producer in the United States, with an economy of $43.5 billion in 2012 (www.cdfa.ca.gov/statistics/) and more than 200 crops producing more than half of the nation's fruits and vegetables. Of these crops, almonds have the highest economic base ($3.87 billion in 2011) and the most acreage planted (870 000 acres in 2012; www.nass.usda.gov/Statistics_by_State/California/Publications/Fruits_and_Nuts/201305almac.pdf). Water use is reported to range between 1020 and 1170 mm yr^{-1} (Sanden 2007). Thus, there is a significant and urgent need to reliably maintain current almond production while using less water. During periods of drought, such as in the droughts of 2007, 2008, and 2009, surface water allotments were significantly reduced to accommodate other uses (Fereres and Soriano 2006; DWR 2009).

Agricultural production in California is possible because of the vast water infrastructure network of reservoirs, groundwater basins, and local and regional water conveyance systems. Nonetheless, California's agriculture is especially vulnerable to water shortages because of its dependence on the winter snowpack, which varies by orders of magnitude between years. Hayhoe et al. (2004) predicted a 60%–90% decrease in the winter "snow water equivalent" snowpack in the Sierra Nevada by 2090 because of global warming, which will profoundly change the timing and intensity of winter and summer surface water flows (Knowles and Cayan 2002; Pimentel et al. 2004).

We address the question of agricultural vulnerability by examining the spatial and temporal patterns of water demand in relation to cropping patterns. Currently, additional knowledge is needed for most crops regarding the timing and magnitude of statewide water demand. Also, knowledge is limited on how timing and insufficient water application affects yield, especially in perennial crops, where past management significantly alters production in subsequent years. Although water deliveries are known, the amount lost to evaporation and leaching beyond the root zone is not fully understood. Without metered well pumps, the amount of additional water used is poorly understood. Various methods have been employed to estimate actual evapotranspiration, the primary force in agricultural water consumption. The California Resource Agency's Department of Water Resources developed crop coefficients to convert "potential evapotranspiration" to actual evapotranspiration (ETa) during the 1970s through 1990s for most crops in California (Allen et al. 1998). The concerns now are that the coefficients do not adequately represent the evapotranspiration rates for today's genotypes.

To provide spatial estimates of ET, the use of remote sensing data products in combination with modeling approaches has been developed by many researchers for more than 30 yr (Jackson et al. 1977; Jackson et al. 1987; Seguin 1989). ET algorithms based on remote sensing data products are comprehensively reviewed and discussed by Gowda et al. (2007), including a summary of the benefits and drawbacks of each algorithm. Kalma et al. (2008) review approaches that use remotely sensed temperature and discuss why certain models are best

applied over specific land cover types or specific disciplines, such as hydrology, for example.

As in most ET-related energy balance models, ET is determined from the residual latent energy (LE) of the surface energy balance budget. Recent approaches to ET modeling include 1) Mapping Evapotranspiration at High Resolution with Internal Calibration (METRIC; Trezza 2002; Allen et al. 2005, 2007), 2) Surface Energy Balance for Land (SEBAL; Bastiaanssen et al. 1998), 3) a two-source energy balance model (TSM; Norman et al. 1995), 4) an aerodynamic temperature-based model (Chávez et al. 2005), 5) an analytical land atmospheric radiometer model (ALARM; Suleiman and Crago 2002), and 6) the Atmosphere–Land Exchange Inverse (ALEXI) model (Anderson et al. 1997, 2007). Allen et al. (2005, 2007) developed the METRIC model, fundamentally rooted in SEBAL (Bastiaanssen et al. 1998), where both models use a near-surface temperature gradient. While models like METRIC and SEBAL are attractive because of their large spatial detail appropriate for subfield mapping, these models are subject to error from selecting inappropriate pixels used for scaling temperature data. Van der Tol and Parodi (2012), for example, state that the remote estimation of ET is still very much custom-made and that it requires specific skills, with the result that the operational dissemination of remote sensing evapotranspiration products still lags behind that of other widely available water cycle components. Actual ET is the last remaining component of the terrestrial water cycle not directly measured from space.

This study introduces a model framework for predicting current and future water and energy fluxes within spatial scales usable by growers and land managers. Many investigations conducted over the past decades established empirical relationships from ground-based observations, such as eddy covariance surface flux studies. These relationships were widely used to develop and improve surface–vegetation–atmosphere transfer (SVAT) models. However, to extend any type of surface measurement, such as eddy covariance, to these high-resolution spatial scales, observations should be coupled to a sophisticated model. This modeling framework demonstrates that an extension of local regression is possible using a state-of-the-art land surface scheme based on micrometeorological theory and observations.

Measurements of surface energy exchange are too complex and costly to be deployed with sufficient spatial coverage necessary for irrigation management. Therefore, it is unlikely that in the near future, this mismatch in spatial scales will be resolved by using more in situ micrometeorological measurements. Spatial maps of crop evaporation (ETo) based on interpolation of meteorological data from stations in combination with remotely sensed incoming solar radiation (Hart et al. 2009) increase the spatial resolution but still suffer from shortcomings intrinsic to interpolated meteorological fields.

While the ability of SVAT schemes to predict ET has made significant progress from the first-generation models, such as simple biosphere (SiB; Sellers et al. 1986) and biosphere–atmosphere transfer scheme (BATS; Dickinson et al. 1986), to the inclusion of snow physics and hydrology in second-generation models, such as the Noah land surface model (LSM; Ek et al. 2003; Barlage et al. 2010; Livneh et al. 2010), and the inclusion of dynamic phenology in third-generation models, such as the Community Land Model (CLM) scheme (Bonan et al. 2002; Dai et al. 2003; Lawrence et al. 2011), we still find large differences between models when these schemes of varying degrees of complexity and surface parameterization are applied across different land use types and, ultimately, to continental and global scales (Jiménez et al. 2011; Mueller et al. 2011). Vinukollu et al. (2011) state that despite the critical role that evaporative processes play in the climate system, including coupling the surface with the atmosphere and links in the water, energy, and carbon cycles, a long-term, high-fidelity reference dataset for ET consistent with other surface data products [such as Global Energy and Water Cycle Experiment (GEWEX)] is still lacking.

Landscapes are heterogeneous on many spatial scales and are rarely uniform within multikilometer grid scales used to assess regional and global surface fluxes. The dominant scales for spatial variability in surface energy fluxes cannot be found by simply scaling up input fields that characterize the landscape, such as soil moisture, albedo, and canopy height. This is due to the inherent nonlinearity of the surface energy balance to surface characteristics (Raupach and Finnigan 1995) and the interlayer within-canopy plant interactions.

Similarity theory, like the Monin–Obukhov similarity theory (MOS), predicts flux variables based on repeatable characteristics in the boundary layer and generally assumes flat, homogeneous surfaces with no vertical extent. MOS is widely used to parameterize surface layer models and is fundamental to our understanding of surface layer processes. However, the impacts of real-world heterogeneity, especially within the vertically diverse roughness layers, on similarity theory predictions remain poorly understood because of the complexity of the problem.

This fundamental question regarding spatial variation in biospheric evapotranspiration has immense practical implications on irrigation practices in times of water scarcity. Although both remote sensing and numerical models are commonly used, traditional simple surface layer schemes in regional and global models are likely to amplify errors in partitioned surface energy budgets.

These errors are due to the nonlinear scaling relationships and significantly impact the simulations of regional energy budgets and atmospheric conditions.

We test the hypothesis that the vertical canopy structure, coupled with horizontal variation in the vertical structure that is associated with ecosystem type, has a strong impact on landscape evapotranspiration. The practical result of testing this hypothesis with the linked Advanced Canopy–Atmosphere–Soil Algorithm (ACASA)–Weather Research Forecast (WRF) model, if demonstrated true, is a new method to obtain increased accuracy of regional evapotranspiration estimates. To test this hypothesis, we applied the ACASA–WRF model at high spatial resolution to a region of almond orchards in the southern San Joaquin Valley of California, north of the city of Bakersfield. ET estimates over agricultural crops are generally referred to as crop evapotranspiration (ETc). Almonds are the top agricultural export for the state of California, with a 2010 yield of 740 000 t, accounting for roughly 95% of U.S. production and 80% of the total worldwide production throughout the last decade (Almond Board of California 2012). Steady improvements in cultural practices, including nutrients and irrigation, has increased almond yields over the past decade by about 80 kg ha^{-1} yr^{-1} (USDA 2010). At the same time, the overall bearing acreage of almonds has steadily increased to become the most widely planted crop in California, with approximately 330 000 ha in 2010 (USDA 2011). Assuming orchards require irrigation of 1370 mm, this equals approximately 4.5 km^3 of irrigation applied water per growing season. Given periodic water shortages, better management of limited water resources by more efficient crop monitoring could become increasingly important.

Improving water use efficiency is one of several answers to water issues facing California. Availability of water from surface sources fluctuates with recurring droughts associated with quasiperiodic weather cycles like the El Niño–Southern Oscillation (ENSO) and the Pacific decadal oscillation (PDO), which may intensify given climate change projections for California (Gutowski et al. 2008; Kunkel et al. 2008). During drought periods, water allotments to agricultural irrigation districts are already severely curtailed because preference is given to other water use demands (Fereres and Soriano 2006). The most recent droughts in 2007, 2008, 2009, and 2010 reduced water allocations by 70% from the State Water Project (DWR 2009).

This study applied the fully coupled version of ACASA–WRF model to simulate ET over the southern San Joaquin Valley at the regional scale. Motivation for coupling WRF with ACASA was to simulate reproducible generalizations of ET at varying spatial and temporal scales. This high-resolution predictive weather modeling will lead to new tools for growers and other stakeholders to improve irrigation efficiencies.

2. Model description

a. The ACASA model

Current research has coupled the WRF model with the University of California, Davis, ACASA model. ACASA is a multilayer micrometeorological ''column physics'' numerical scheme that describes the surface layer, including aspects representing terrestrial biosphere; turbulent microenvironment; and associated heat, water vapor, momentum, and carbon dioxide exchanges (Meyers 1985; Meyers and Paw U 1986; Pyles 2000; Pyles et al. 2003; Xu 2012; Blečić et al. 2013).

A surface layer scheme is included in WRF that is similar to the National Centers for Environmental Prediction (NCEP) community Noah LSM. The ACASA surface layer model is applicable at spatiotemporal scales roughly equivalent to typical WRF surface pixels and AmeriFlux–EUROFLUX micrometeorological measuring towers. ACASA differs from Noah LSM by being a multilayer, higher-order closure turbulence and energy exchange model that includes carbon dioxide exchanges within plant canopies and urban environments. Additional features include soil thermal and hydrological exchange modeling applied to 10 soil layers and as many as 10 subcanopy snow layers, using strategies similar to Noah LSM. Calculations of plant canopy and urban heat cycling include transient diffusion into large stems and trunks and building materials using the same basic diffusion methods used for soil.

Since its original release as a generalized surface layer model (Pyles 2000; Pyles et al. 2000), ACASA has continued to improve with increased reliability and accuracy. The governing equations for ACASA are available in Meyers and Paw U (1987), Paw U and Gao (1988), Paw U (1997), and Pyles (2000); some of these papers present comparisons that establish improved accuracy of this model over simpler models. Recent changes to ACASA are summarized in Marras et al. (2011), Staudt et al. (2010), and Xu (2012), who describe the ability of ACASA to simulate vastly different ecosystem types.

b. The WRF model

WRF is a next-generation community mesoscale meteorology model with support by the National Center for Atmospheric Research (NCAR). It is widely used for both operational air quality and weather forecasting and climate change research (http://wrf-model.org/index.php). In this study the Advanced Research WRF (ARW) core, version 3.1.1 (Skamarock et al. 2008), was used. WRF is a fully compressible, nonhydrostatic model with

TABLE 1. WRF–ACASA coupling variables.

WRF variable name	Description (units)	Source
WRF → ACASA forcing meteorology		
T3D	Air temperature (K)	WRF, lowest layer
QV3D	Specific humidity ($kg\,kg^{-1}$)	WRF, lowest layer
GSW	Downwelling shortwave radiation ($W\,m^{-2}$)	WRF, lowest layer
GLW	Downwelling longwave radiation ($W\,m^{-2}$)	WRF, lowest layer
$(U\_PHY^2 + V\_PHY^2)^{1/2}$	Wind speed ($m\,s^{-1}$)	WRF, lowest layer
P8W3D	Barometric pressure (Pa)	WRF, lowest layer
RAINBL	Precipitation rate ($kg\,m^{-2}$ PBL_timestep^{-1})	WRF, lowest layer
WRF → ACASA surface morphology		
LAI	Leaf area index (green; $m^2\,m^{-2}$)	WRF/MODIS
VCMAX_CLM	Photosynthetic potential ($\mu mol\,m^{-2}\,s^{-1}$)	CLM lookup table
100*Z0BRD	Canopy height (90th percentile; m)	WRF
ALBBCK	Subscale (leaf) visible reflectance (–)	WRF
ALBBCK + 0.1	Subscale (leaf) near-infrared reflectance (–)	WRF
ALBBCK	Ground surface visible reflectance (–)	WRF
ALBBCK + 0.1	Ground surface near-infrared reflectance (–)	WRF
ISLTYP	Soil type and diffusion parameters (–)	WRF
SMCDRY	Air-dry value of soil moisture (volumetric)	WRF
SMCREF	Wilting point soil moisture (volumetric)	WRF
ACASA → WRF forcings (direct and indirect feedbacks that influence WRF meteorology)		
HFX	Sensible (convective) heat flux density ($W\,m^{-2}$)	ACASA
QFX	Water vapor flux density ($kg\,m^{-2}\,s^{-1}$)	ACASA
USTAR	Friction velocity ($m\,s^{-1}$)	ACASA
TKE_MYJ	Turbulent kinetic energy from Mellor–Yamada–Janjić scheme ($J\,m^{-2}$)	ACASA
ALB	Shortwave albedo (–)	ACASA
EMISS	Thermal emissivity (–)	ACASA
TSK	Surface (skin) temperature (K)	ACASA
Q1	Surface specific humidity ($kg\,kg^{-1}$)	ACASA
TSLB	Soil temperature (K)	WRF (initial), ACASA
SMOIS	Soil moisture (volumetric)	WRF (initial), ACASA
SNOW	Snowpack water content ($kg\,m^{-2}$)	WRF (initial), ACASA
T_SSL_SNOWPACK*	Snowpack temperature (K)	WRF (initial), ACASA
T_SSL_STEMS2*	Canopy temperatures–leaves and small stems	WRF (initial), ACASA
T_SSL_STEMS1*	Canopy temperatures–large stems	WRF (initial), ACASA
T_SSL_BLDGS*	Canopy temperatures–buildings	WRF (initial), ACASA
CANWAT	Total canopy water content	0 (initial), ACASA

* Mean values of several ACASA morphological parameters: leaf diameter, leaf drag coefficient, and shortwave radiative transmissivities were set to constant values for all vegetation types because of a lack of WRF values and a relatively low ACASA sensitivity to each.

terrain-following vertical sigma-level coordinates. The ACASA–WRF simulations ran with 28 sigma vertical levels, four soil levels, and four-dimensional data assimilation (FDDA) nudging.

c. *ACASA–WRF coupling*

ACASA was driven with the following set of input variables, mainly surface morphology data and WRF meteorological conditions at the lowest terrain-following sigma level, which are provided by WRF for each ACASA time step. These include air temperature, pressure, specific humidity, precipitation rate and phase, downwelling solar [photosynthetically active radiation (PAR) + near-infrared radiation (NIR)] and terrestrial [thermal infrared radiation (TIR)] radiation flux density, and bulk air CO_2 concentration (here assumed constant at 392 ppm for 2008) at the first WRF sigma layer. In addition to WRF meteorological data, most morphological parameters needed to describe each point were also provided by WRF and varied by land use type (Xu 2012; R. D. Pyles et al. 2014, unpublished manuscript; Table 1).

ACASA is coupled to WRF using the same surrounding architecture used for Noah LSM. In WRF, the planetary boundary layer (PBL) and surface calculations are divided into three computational regimes: 1) the PBL proper, extending above the surface sublayer (SSL) to any arbitrary height, depending on accompanying dynamics, with the PBL height changing spatiotemporally; 2) the SSL; and 3) the surface itself, including soil, water, and/or snow. Regimes 2 and 3 are considered active ''beneath'' WRF sigma layer 1with surface layer exchanges (fluxes) occurring between each. The Noah LSM regime includes both the surface and the SSL

abstracted to one imaginary flat plane, with heat, moisture, and momentum fluxes contributing to changes in the time tendencies of temperature, water vapor, and wind velocities at lower atmospheric layer (sigma-1). WRF sigma-1 meteorological values drive Noah LSM, which then provides the fluxes (feedbacks) to the WRF PBL and radiation routines at sigma layer 1.

The surrounding Noah LSM coupling architecture mentioned above is also used for ACASA. The set of driving meteorological variables and associated fluxes between the SSL and WRF proper are summarized in Table 1. However, in contrast to Noah LSM and similar models, ACASA resolves vertical variations within the canopy (subscale effect) that each contributes through process-based physiological and turbulent transport dynamics to the total set of fluxes and conditions needed to drive WRF in nonlinear ways. The logic behind using this methodology is illustrated by the following: thermal emissions are proportional to the fourth power of temperature. Therefore, using a single, average temperature value to calculate the total (radiative) thermal emission flux for each pixel can yield much different results than would occur using explicit methods of integration involving resolved subscale component temperature estimates. The same is true for the set of SSL water vapor, momentum, and sensible heat transports, as well as "bulk" surface temperature and humidity values that are also required by WRF to function properly. Furthermore, by representing surface physics and physiology using multiple vertical layers, ACASA provides a distinct advantage over most simpler models, which often represent the whole system as one layer. This can be illustrated by considering a snowpack shaded by a forest canopy, where the leaf temperatures can be tens of degrees warmer than the snowpack.

3. Experimental method

a. Input data

1) NCEP–NCAR REANALYSIS PRODUCT

This study used the NCEP North American Regional Reanalysis (NARR) data to provide initial conditions for all domains and boundary conditions for the mother domain in the ACASA–WRF simulations. The data for this study are from the Research Data Archive (RDA), which is maintained by the Computational and Information Systems Laboratory (CISL) at NCAR. NCAR is sponsored by the National Science Foundation (NSF). The original data are available from the RDA (http://rda.ucar.edu) in dataset number ds608.0 (NCEP 2012).

NARR results were interpolated to NCEP grid 221 with 32-km resolution and 29 pressure levels before the data were archived. The reanalysis was produced using the NCEP Eta Model with a resolution of 32 km and 45 vertical layers. The input data included all observations used in the NCEP–NCAR Global Reanalysis project with additional data on precipitation, Television Infrared Observation Satellite (TIROS) Operational Vertical Sounder (TOVS) 1B radiances, atmospheric profiles, and land surface and moisture data. The NARR output analyses data are available in 3-h intervals.

2) LEAF AREA INDEX

In coupling ACASA to WRF, we also added the ability to input leaf area index (LAI) grid point values either from observed data or the previous method of assigning values according to vegetation type in a look-up table (http://igoroliveira.org/wrf/wrf_lai/WRF_Model.html). We utilized the improved Moderate Resolution Imaging Spectroradiometer (MODIS) LAI product (Yuan et al. 2011) based on the MODIS 8-day LAI composites from 2000 to 2009 with spatial resolution of 1 km^2. For this study, we resampled the data to cover California for 2008. The WRF Preprocessing System (WPS) converts the MODIS LAI time series to a monthly LAI value passed by WRF to the ACASA land surface scheme during simulation.

3) CALIFORNIA AUGMENTED MULTISOURCE LAND COVER DATA

This study used California Augmented Multisource Land Cover (CAML) data for 2006 (http://atlas.resources.ca.gov/ArcGIS/rest/services/Environment/CAML/MapServer) to produce WRF land use index values for the high-spatial-resolution domains. CAML data cover all of California and are available as a 100-m-resolution raster dataset. The CAML data include categories for agricultural land cover types as well as urban boundaries complete to 2006. The agricultural cover mapping was developed from the type categories within the California Wildlife Habitat Relationships system (www.dfg.ca.gov/biogeodata/cwhr/wildlife_habitats.asp), Department of Water Resources (DWR) Land and Water Use (www.water.ca.gov/landwateruse/lusrvymain.cfm) and the Department of Pesticide Regulation pesticide-use crop information. Urban land use was identified by combining the 2002 map urban boundaries in the Department of Conservation Farmland Mapping Program (www.conservation.ca.gov/DLRP/fmmp/Pages/Index.aspx) and the 2001 National Land Cover Dataset (Homer et al. 2007; www.mrlc.gov/nlcd2001.php). We translated the CAML land cover classes to the U.S. Geological Survey (USGS) 33 scheme specified for WRF input structure (www.mmm.ucar.edu/wrf/users/docs/user_guide_V3/users_guide_chap3.htm#_Land_Use_and).

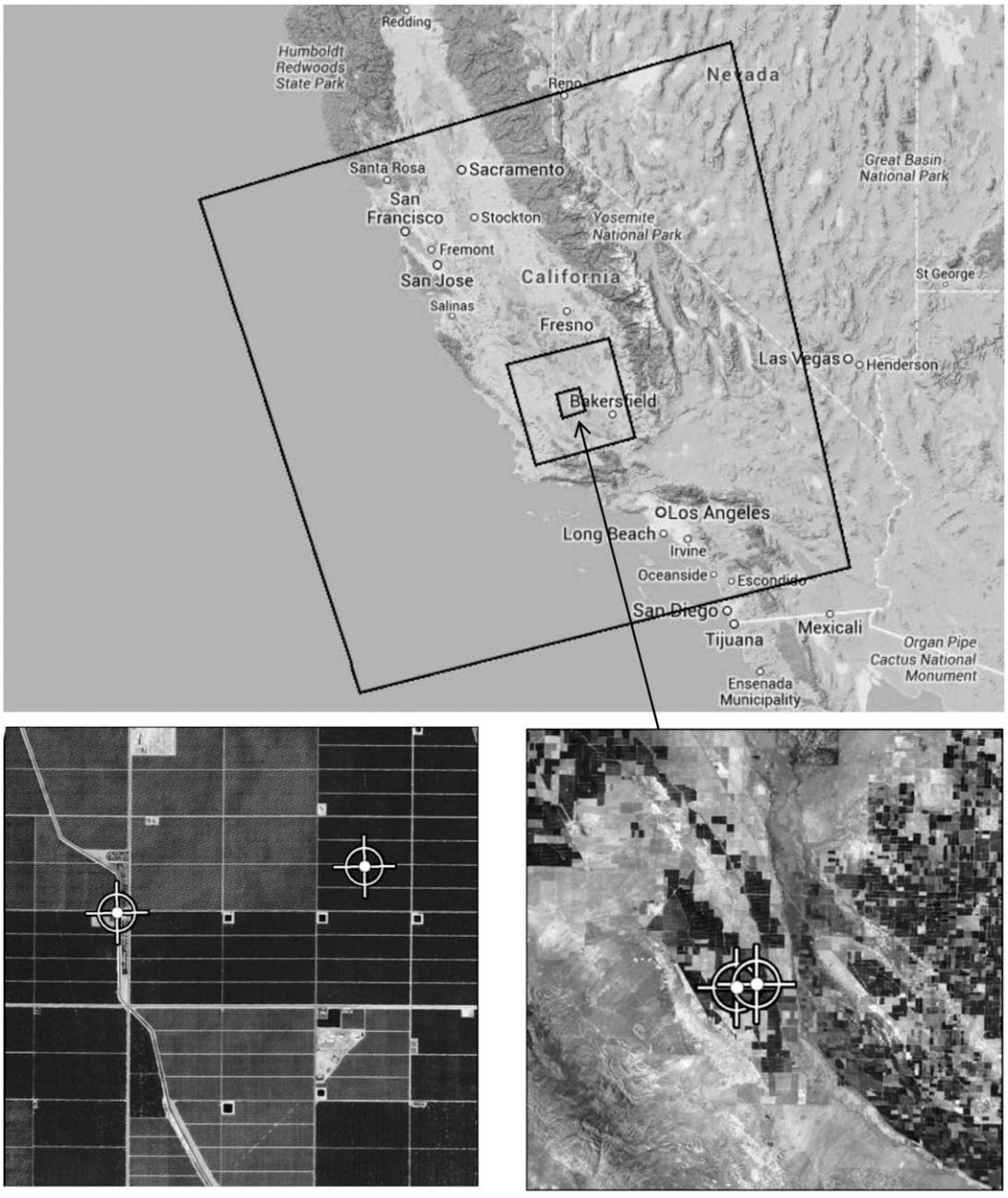

FIG. 1. (top) Location of the three ACASA–WRF domains d01, d02, and d03 (8-, 2-, and 0.5-km grid size, respectively) within California. (bottom right) A Landsat scene showing d03 (40 × 40 km extent) illustrates the patchwork of irrigated crop land (dark) surrounded by dry land (light) areas. (bottom left) The high-resolution scene shows the orchard blocks in the center of the domain.

b. Model domains

This study covered the portion of the almond growing season from 20 March through 30 September 2008 using a sequence of three nested, fully coupled spatial domains centered on the Belridge orchard eddy covariance (EC) tower (35.6°N, 119.3°W; see Fig. 1). The horizontal grid spacing of the largest domain (d01) was 8 km × 8 km. The spacing of the subsequent nested domains were 2 km × 2 km (d02) and 0.5 km × 0.5 km (d03). The horizontal resolution ratio between each nested domain to its parent was 1:4. The ratio from NARR data to the ACASA–WRF parent domain was also 1:4. Domain 3 is presented here (Fig. 1). We conducted a sequence of monthly simulations using ACASA–WRF to accommodate the finescale simulations with a spinup time of 2 days.

Domain d03 extended 40 km × 40 km (80 × 80 grid cells) to encompass irrigated orchards and open dry

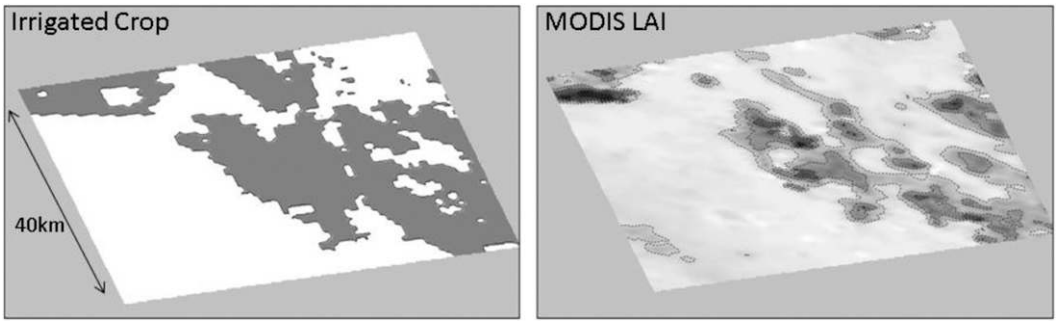

FIG. 2. (left) Irrigated crop cover type (dark gray) in d03 and (right) MODIS LAI for June 2008 shown as static input fields from the ACASA–WRF model output.

grasslands on the west side of the southern San Joaquin Valley. Distribution of land use, LAI, and land use type (LUINDEX parameter) in ACASA–WRF are shown in Fig. 2. The NARR data provides initial conditions for all three nested domains in this experiment, while boundary conditions from NARR are provided only for domain 1 throughout the simulation. The nested domains (d02 and d03) receive their boundary conditions from the mother domain (d01 and d02, respectively).

c. *Ground observation dataset description*

1) BELRIDGE ALMOND ORCHARD SITE

Ground observation data were collected at an almond orchard located south of the town of Lost Hills, California (35.51°N, 119.67°W). The orchard is owned and operated by Paramount Farming Company (PFC), Bakersfield, California, which has cooperated for many years with the University of California in conducting intensive nutrient and water experiments in deciduous nut tree crops. The mature orchard block consisted of almond [*Prunus dulcis* (Mill.) D. A. Webb] production variety Nonpareil (50%) and pollination variety Monterey (50%) planted 9 yr (1999) before this study. In this region, almond trees typically flower in early to mid-February, leaves appear in early March, and they are ready for harvest in late August for Nonpareil and late October for Monterey (Almond Board of California 2012).

The climate in the San Joaquin Valley is hot, semiarid Mediterranean type, characterized by hot dry summers and mild winters. Annual average temperature is 17.3°C, with an average annual precipitation of 134 mm, almost entirely during the winter months, November–April. The average annual reference ETo is 1496 mm. Climate data were obtained from the California Irrigation Management Information System (CIMIS) Belridge Station (No. 146) (www.cimis.water.ca.gov/cimis/frontStationDetailInfo.do?stationId=146).

2) EDDY COVARIANCE

Eddy covariance measurements of evapotranspiration provide a direct measurement of surface energy budget fluxes into and out of a plant canopy and are currently considered the most reliable method for measuring ET over areas of hundreds of square meters (Drexler et al. 2004). While we cannot calibrate eddy covariance systems as a whole to get absolute overall accuracy, the general accuracy of EC measurements is estimated to be in the range of 5%–30% (Hollinger and Richardson 2005; Baldocchi 2003). Possible error sources for ET include factors such as the surface energy balance closure error (Foken 2008; Mahrt 2010).

We evaluated the ACASA–WRF model estimates of ETc against measurements of LE converted to ETc at the EC tower located in the center of the ACASA–WRF d03 domain. The tower pixel x–y location within the domain grid was 33, 47 in the 80×80 cell domain. The EC tower system (McElrone et al. 2013) was established in early 2008 within the Belridge almond orchard. The EC system is part of an ongoing program by the DWR to reevaluate existing recommended estimates for crop ETc coefficients (Kc) used to calculate ETc from CIMIS ETo measurements. Each tower EC system consists of two fine wire chrome-constant thermocouples (FW3 with 76.2-μm diameter; Campbell Scientific, Inc., Logan, Utah), Young Model 81000 Ultrasonic Anemometer (R. M. Young, Traverse City, Michigan), REBS Q7 net radiometer (REBS, Inc., Seattle, Washington), several REBS HFT3 soil heat flux plates (REBS, Inc.), and several soil temperature probes (Campbell Scientific). Setup and data acquisition methods are described by Snyder et al. (2007). EC data preprocessing and quality control was done via validated software developed by Snyder (R. L. Snyder 2011, personal communication).

The EC system used at the Belridge site was developed by R. L. Snyder and colleagues and was extensively tested

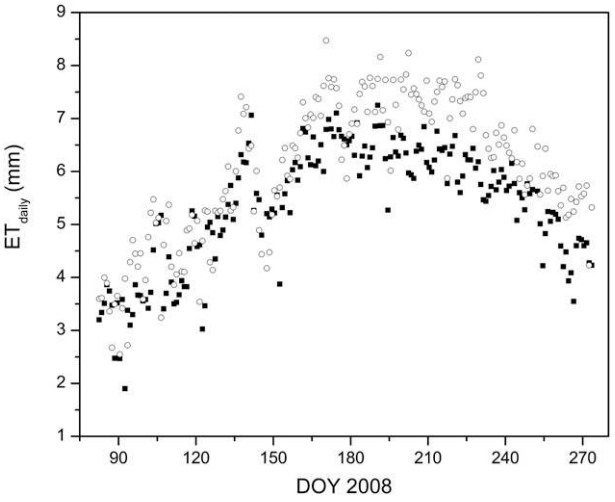

FIG. 3. Daily ET for the ACASA–WRF simulation for the tower pixel (solid circles) and observations from the Belridge EC (open circles).

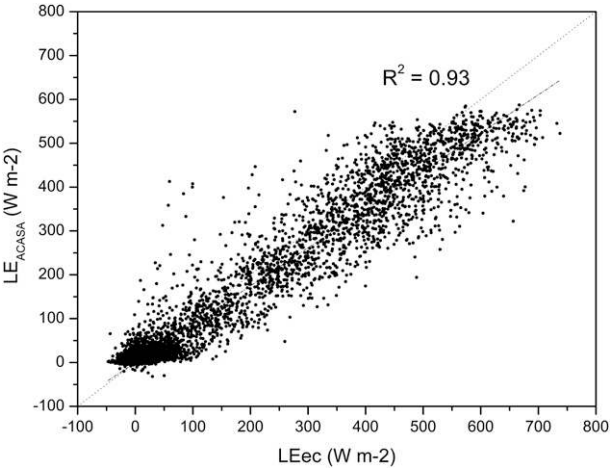

FIG. 4. Hourly fluxes of LE: ACASA–WRF plotted against observations from the Belridge EC tower with the linear regression shown.

for application in agricultural systems of California (Snyder et al. 2008; Castellví and Snyder 2010). For example, Castellví and Snyder (2010) evaluated the performance of the EC system over an irrigated grass canopy against a weighting lysimeter at Five Points, California, located close to the site of this study. For LE derived from eddy covariance, Castellví and Snyder (2010) found that $LE_{EC} = 0.97 \times LE_{lysimeter} - 2.0\ (W\ m^{-2})$ and $R^2 = 0.98$.

4. Results and discussion

a. *Comparison of model estimates of LE and ET with observations*

Shown in Fig. 3 are the time series of daily ET at Belridge tower pixel for both ACASA–WRF model estimates (filled symbols) and EC observation (open symbols) from the start of EC data collection on day of year (DOY) 82 through the season, DOY 273, 2008. This spans the main growth and irrigation period to the harvest when irrigation is stopped for several weeks. Generally, the modeled ET results and observations follow the same seasonal pattern, with maximum ET during the summer. More illustrative of the sensitivity of the model is the parallel tracking of observations with a pronounced peak and dip in ET before and after DOY 150. A slight low bias (less than 15% of observed) is seen in the summer pattern after DOY 180 by the model ET estimates. However, Fig. 4 plots the hourly LE observations (measured by EC) against ACASA–WRF LE estimates and shows good agreement across the entire range of LE values. Linear regression of the model LE estimates versus observed LE produces a slope of 0.87 with an $R^2 = 0.93$; the model explains greater than 90% of observed variation in LE. Generally, the model estimates follow the 1:1 line to the observed, but the underestimation of LE (lower slope coefficient) might be due to decreasing MODIS LAI during the midseason while observed LE continued to increase in the range of high values.

Average daily ET based on an 8-day running mean improved the correlation between modeled and observed ET at the tower pixel (shown in Fig. 5, top) with significantly reduced scatter. Linear regression of modeled versus observed 8-day average ET yielded a comparable slope of 0.82 ($R^2 = 0.93$).

b. *The impact of LAI on the seasonal course of ET*

The inclusion of MODIS LAI as an ACASA–WRF input field greatly improved the ability of ACASA–WRF to simulate the seasonal course of ET. However, there are limitations to the accuracy of LAI produced with MODIS data. Spatial errors are the greatest source of errors in highly heterogeneous areas. The orchard area is homogenous, with a long fetch of similar canopy, greater than 7 km to a dramatic change at the boundary with the dry grassland. Within grasslands, the LAI was again consistent for greater than 10–15 km. There are minor but additional LAI errors generated when data pass through the WRF WPS to ACASA–WRF. The WPS process reprojects MODIS LAI values to the model grid and averages over all neighboring points contained in each model pixel.

The approximate seasonal course of LAI for the ACASA model at the tower pixel is shown in Fig. 6. The peak of the MODIS LAI in the main growing season (1.2) is within the observational uncertainty of field

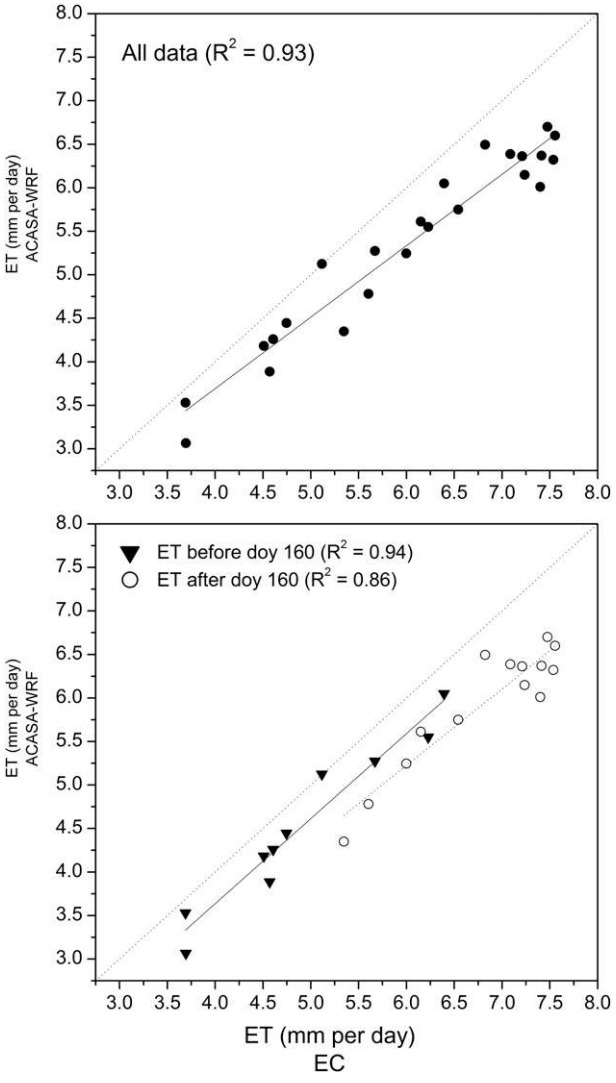

FIG. 5. Average 8-day values of daily ET: ACASA–WRF plotted against observations from the Belridge EC tower. (top) All data and (bottom) data separated into two populations (before and after DOY 165) with the linear regressions for all three cases shown.

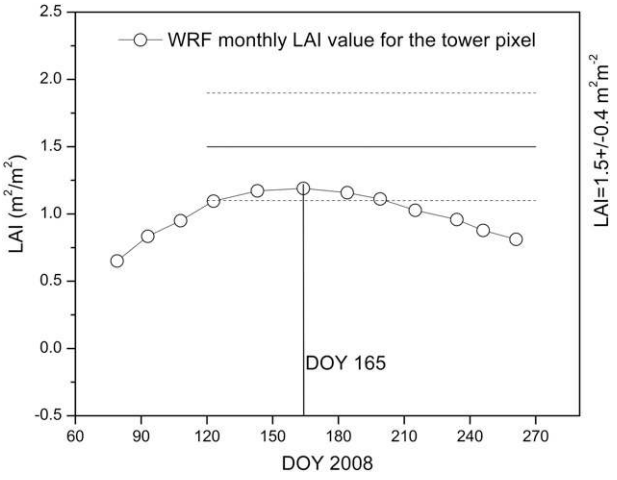

FIG. 6. Monthly LAI used in the WRF simulations at the pixel containing the flux tower site (circles) and ground-based maximum growing season LAI (1.5 ± 0.4) shown as the solid horizontal line with error bars shown as dashed horizontal lines for the Belridge almond orchard.

measurements at the Belridge site (1.5 ± 0.4). However, the MODIS LAI value is on the low side of the ground-based estimate. This overall low bias of MODIS LAI compared to field measurements will contribute to the observed low bias in the ACASA–WRF ET estimates. The spatial distribution of LAI in Fig. 3 for June 2008 shows significant variation both between crop and non-crop lands and within similar crop lands. The overall range of LAI in d03 is 0.0–2.0. Furthermore, MODIS LAI shows a steady reduction in LAI between peak (~DOY 165) and harvest (~DOY 240) that is not observed on the ground. This systematic decrease likely introduced an additional reduction in modeled ET for that period. To evaluate the impact of this midseason decline in LAI, we divided the 8-day ET data into two subsets, all data before and after DOY 165. In Fig. 5 (bottom), linear regression of model results versus observed data from before DOY 165 (filled triangles) improved the model estimation slope to 0.98 ± 0.08 with an R^2 of 0.94, while linear regression for the period after DOY 165 (open circles) yielded an improvement of the fitted slope to 0.88 ± 0.10, with a slight decrease in R^2 to 0.86. These results indicate the model performed better during the first half of the simulation period, with a slope not significantly different from 1.0, while explaining 94% of variation in the 8-day ET observations. After DOY 165, the MODIS LAI decreases steadily (Fig. 6) from 1.20 to 0.87 by the end of August, representing a significant increase in soil background. Field observations do not support any significant leaf loss by the almond trees before harvest near September. However, one explanation for the apparent decline in LAI is that the increasing weight of nuts through the season bends the branches downward, opening the crown geometry and likely reducing the calculated MODIS LAI. In California, almonds retain their leaves well into October or until the start of cooler winter temperatures. This indicates that the same number of leaves are mixed in the pixel but were spread over a greater ground area. This apparent decline demonstrates a nonlinear effect due to increased exposure of soil background on the calculation of LAI. Since WRF–WPS contributes the MODIS LAI to ACASA, this apparent seasonal reduction in LAI caused a small decrease in model-estimated ET after DOY 165, increasing the ET low bias as shown in Fig. 5 (bottom). Adjusting the MODIS LAI in the WRF

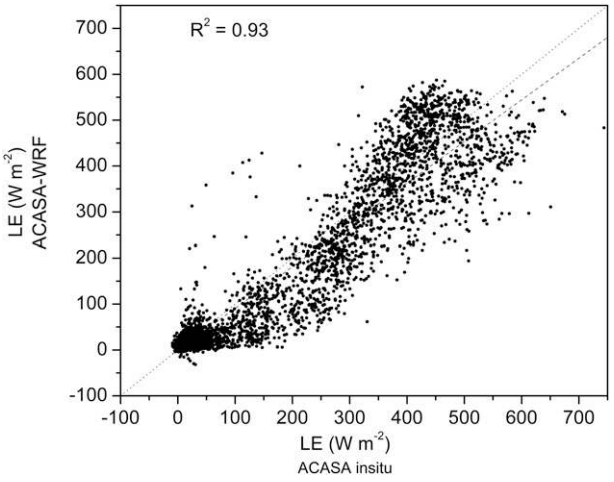

FIG. 7. Hourly fluxes of LE: ACASA–WRF plotted against a simulation of the stand-alone version of ACASA for the Belridge almond orchard (data from Falk et al. 2012, manuscript submitted to *Hydrol. Processes*) with the linear regression shown.

WPS input data to correct for this apparent seasonal decline and the overall low bias in LAI is expected to improve the performance of ACASA as a land surface model within WRF.

c. *Seasonal total ET for the tower pixel*

Over the entire season, the performance of the new ACASA–WRF model was well correlated to LE and ET measurements. The coupling of ACASA–WRF reduced ACASA accuracy to simulate ET at the Belridge site only slightly compared to the uncoupled ACASA predictions while providing ET estimates over an area of 1600 km^2 at 0.5-km resolution. The seasonal ET estimate of the stand-alone version of the ACASA model (1180 mm) when driven solely with local meteorology, site-specific LAI, and other model parameters was previously shown to be within 2% of observed seasonal EC ET (1157 mm). A direct comparison of half-hourly LE estimates between the ACASA–WRF model and the ACASA stand-alone model produced a linear regression with a slope of 0.91 and R^2 of 0.93 (Fig. 7). The ACASA–WRF model estimate for growing season ET (1028 mm) was within 11% of the measured ET for the same period (20 March through 30 September).

d. *Spatial variability of ET*

The nested simulations of ACASA–WRF also produced hourly LE estimates for the 1600 km^2 area (6400 separate model grid points in domain d03). Within the mixed land covers, the simulation domain contained irrigated orchards, dry grassland, small towns, and oil production areas classified in WRF as urban. Figure 8 shows the seasonal course of ET across the landscape in the form of maps for total monthly ET for the period of April–August 2008 in the first five panels. Clearly visible is the stark contrast of very high values of ET over irrigated croplands with high LAI against the dry surrounding landscape. At this interface, we observed significant shift of ±20% of ET along orchard pixels adjacent to grassland. This can be explained by the "clothesline effect," where hot dry air advects into a well-watered crop canopy and drives ET increase. Some of the variation can also be explained by variations in LAI; that is, irrigated crop areas with lower LAI contribute less ET than areas with higher LAI (Fig. 2).

The map of seasonal total ET shown in the last panel of Fig. 8 is composed of the monthly ET shown in first panels of Fig. 8 plus the 10 days of March 2008. Model estimates for seasonal ET for the central orchard area range from 900 to 1100 mm (shown in blue in the last panel of Fig. 8). As reported above, this total compares well to the Belridge EC tower ET of 1036 mm while providing detailed pixel variation and expected variability of seasonal ET over the area of interest.

5. Conclusions

Here we presented an application of a fully coupled version of ACASA with the WRF model to simulate spatially distributed ET over regional scales. The combination of additional remotely sensed data such as MODIS LAI and CAML data as input for the ACASA–WRF simulations is a crucial step toward better spatial modeling of land surface fluxes. The motivation for coupling WRF with ACASA was to simulate reproducible generalizations for ET on varying spatial and temporal scales. The study area and focus of this study contains irrigated agricultural crops, specifically irrigated almond orchards. While 2008 was a drought year in California overall, the crops were irrigated to full ETc potential. The EC tower at the site did not find differences in ETc between 2008 and 2009, for example. Over 90% of available water at the site is provided via surface water irrigation. Less than 10% of water is typically provided by precipitation, which falls during the dormant period of the orchard growth cycle. Analysis of longer-term monthly ETo data from the CIMIS Belridge station gives the 11-yr average from 2000 to 2010 for the period of April–August as 960 mm (950 mm for 2008 only). Thus, 2008 was not an unusual year for the irrigated orchard but a typical one for expected water demand and irrigation at the site.

When compared to observed eddy covariance ET, the model performed well over the course of a growing season. The model performance tracking ET throughout the season was good, but modeled ET values were slightly

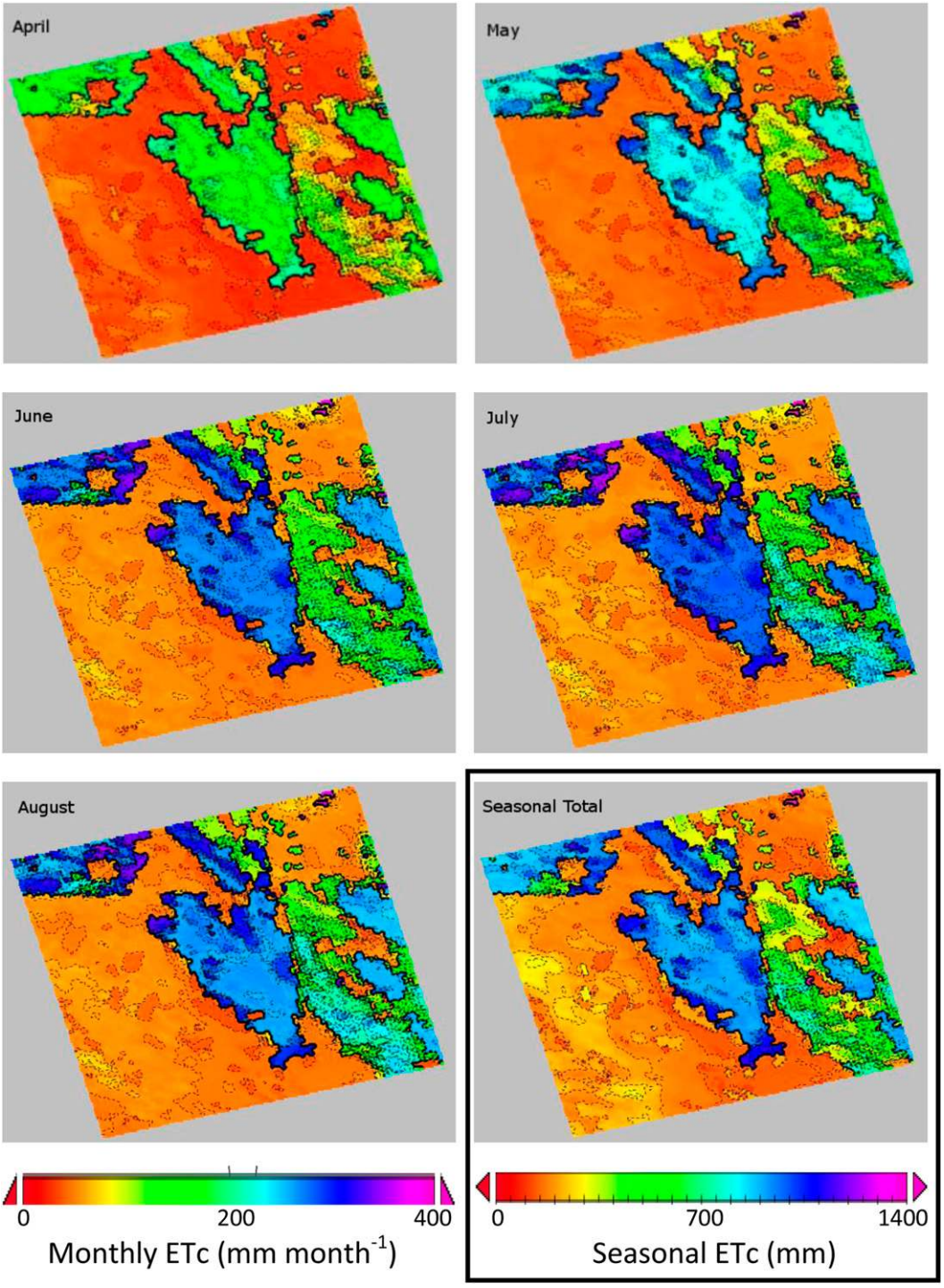

FIG. 8. Monthly and seasonal total maps of ETc for d03 centered on the Belridge orchards. Shown are complete months from the ACASA–WRF simulations for the period April–August 2008 (scale at bottom left) and seasonal total ET (in the bottom-right panel).

lower than observed estimates. This difference was likely due to MODIS LAI values (1.2) being in the lower range of the observational uncertainty of ground-based LAI (1.5 ± 0.4). This low bias increased when MODIS LAI significantly declined after it peaked around DOY 165. However, the change in MODIS LAI also illustrates the sensitivity of ACASA to varying LAI. Despite the problem with declining LAI near the end of the

growing season, the seasonal total ET estimated by ACASA–WRF was still within 11% of the measured total. This result was well within the assumed uncertainty of EC measurements of 15%–30%. Within the experimental domain, ACASA–WRF predicted variation in ET from orchard to orchard, driven by both variation in LAI and local microclimate. We observed a clothes line effect of higher ET when the landscape abruptly transitioned from dry land to irrigated crop land.

Our study introduced a very detailed, physically based LSM coupled to WRF for agricultural irrigated systems that allowed us to address some of the crucial issues that water-resource managers and growers in California will face in the future. ACASA–WRF in this study clearly shows its validity and utility as an advanced tool to provide high-resolution spatial estimates of ET over long periods with a high degree of accuracy and minimum external inputs.

In the future, the WRF–ACASA model system will benefit from better overall parameterization of land surface characteristics and vegetation parameters such as reflectance, canopy structure, and leaf physiology. For example, if we can improve upon the estimates of MODIS LAI, we can provide a better representation of the seasonal changes in phenology within the regional model. Improvements in LAI estimates are likely to be reached by combining ground-based measurements with weather satellite data or from higher-spatial-resolution satellite imagery such as Landsat (Zarate-Valdez et al. 2012). Other parameters of canopy structure (such as canopy height and LAI distribution with throughout the canopy) can be obtained from airborne and satellite-based instruments, such as radar and lidar (Simard et al. 2011). An increased number and accuracy of land use classifications will improve the ACASA–WRF model scheme by differentiating between different crops and will recognize additional natural ecosystems. Once these datasets become routinely available over large spatial areas, they can be incorporated in the input data fields of the ACASA–WRF model and can replace lookup table values.

Climate change simulations for the West Coast region, including California, generally predict higher temperatures and shifts in precipitation timing, phase, and perhaps magnitude. While evapotranspiration generally goes up with temperature, other factors such as higher yield due to increased atmospheric CO_2 concentrations might reduce overall water consumption (Körner 2000). Thus, it is imperative to develop and deploy state-of-the-art micrometeorological models like ACASA as an integral part of models like WRF so that regional models can accurately simulate water use under changing climate and site conditions for a variety of crop types. These models need to supplement existing climate change simulations with global and regional climate model schemes to accurately assess impacts of climate change at a scale relevant to growers, water resource managers, and the public at large.

Acknowledgments. The authors wish to extend our appreciation for research funding from the USDA National Institute of Food and Agriculture, Specialty Crop Research Initiative (Grant 2008-51180-19563). Portions of K.T.P.U's participation in this project were funded by National Science Foundation Prime Award EF 1137306 to the Massachusetts Institute of Technology, secondarily awarded to UC Davis as Subaward 5710003122. Portions of M.F.'s and R.D.P.'s participation in this project were funded by the EU-funded project BRIDGE (Seventh Framework Programme of the European Community/Project Reference 211345) and Italian Ministry of Environment GEMINA Project (Contract 232/2011). Through this research initiative and collaboration of the sponsored investigation, the synergy of complimentary data was possible. In addition, we thank Paramount Farming Company for their continued cooperation.

REFERENCES

Allen, R. G., L. S. Pereira, D. Raes, and M. Smith, 1998: Crop evapotranspiration—Guidelines for computing crop water requirements. FAO Irrigation and Drainage Paper 56, FAO, Rome, Italy, 333 pp. [Available online at www.fao.org/docrep/x0490e/x0490e00.htm.]

——, M. Tasumi, A. Morse, and R. Trezza, 2005: A Landsat-based energy balance and evapotranspiration model in western US water rights regulation and planning. *Irrig. Drain. Syst.,* **19,** 251–268, doi:10.1007/s10795-005-5187-z.

——, and Coauthors, 2007: Satellite-based energy balance for Mapping Evapotranspiration with Internalized Calibration (METRIC)—Applications. *J. Irrig. Drain. Eng.,* **133,** 395–406, doi:10.1061/(ASCE)0733-9437(2007)133:4(395).

Almond Board of California, cited 2012: 2011 almond almanac. Doc. of the Almond Board of California, Modesto, CA, 41 pp. [Available online at www.almondboard.com/AboutTheAlmondBoard/Documents/ALM110600_Almanac2011_LR.pdf.]

Anderson, M., J. M. Norman, G. R. Diak, W. P. Kustas, and J. R. Mecikalski, 1997: A two-source time-integrated model for estimating surface fluxes using thermal infrared remote sensing. *Remote Sens. Environ.,* **60,** 195–216, doi:10.1016/S0034-4257(96)00215-5.

——, ——, J. R. Mecikalski, J. A. Otkin, and W. P. Kustas, 2007: A climatological study of evapotranspiration and moisture stress across the continental United States based on thermal remote sensing. *J. Geophys. Res.,* **112,** D11112, doi:10.1029/2006JD007507.

Baldocchi, D. D., 2003: Assessing the eddy covariance technique for evaluating carbon dioxide exchange rates of ecosystems: Past, present and future. *Global Change Biol.,* **9,** 479–492, doi:10.1046/j.1365-2486.2003.00629.x.

Barlage, M., and Coauthors, 2010: Noah land surface model modifications to improve snowpack prediction in the Colorado

Rocky Mountains. *J. Geophys. Res.,* **115,** D22101, doi:10.1029/2009JD013470.

Bastiaanssen, W. G. M., M. Menenti, R. A. Feddes, and A. A. M. Holtslag, 1998: A remote sensing surface energy balance algorithm for land (SEBAL). 1. Formulation. *J. Hydrol.,* **212–213,** 198–212, doi:10.1016/S0022-1694(98)00253-4.

Blečić, I., A. Cecchini, M. Falk, S. Marras, D. R. Pyles, D. Spano, and G. A. Trunfio, 2013: Urban metabolism and climate change: A planning support system. *Int. J. Appl. Earth Obs. Geoinf.,* **26,** 447–457, doi:10.1016/j.jag.2013.08.006.

Bonan, G. B., K. W. Oleson, M. Vertenstein, S. Levis, X. Zen, Y. Dai, R. E. Dickinson, and Z.-L. Yang, 2002: The land surface climatology of the community land model coupled to the NCAR community climate model. *J. Climate,* **15,** 3123–3149, doi:10.1175/1520-0442(2002)015<3123:TLSCOT>2.0.CO;2.

DWR, 2009: California water plan update 2009. Bull. 160-09, Department of Water Resources, Sacramento, CA. [Available online at www.waterplan.water.ca.gov/cwpu2009/index.cfm.]

Castellví, F., and R. L. Snyder, 2010: A comparison between latent heat fluxes over grass using a weighing lysimeter and surface renewal analysis. *J. Hydrol.,* **381,** 213–220, doi:10.1016/j.jhydrol.2009.11.043.

Chávez, J., C. M. U. Neale, L. E. Hipps, J. H. Prueger, and W. P. Kustas, 2005: Comparing aircraft-based remotely sensed energy balance fluxes with eddy covariance tower data using heat flux source area functions. *J. Hydrometeor.,* **6,** 923–940, doi:10.1175/JHM467.1.

Dai, Y., and Coauthors, 2003: The Common Land Model (CLM). *Bull. Amer. Meteor. Soc.,* **84,** 1013–1024, doi:10.1175/BAMS-84-8-1013.

Dickinson, R. E., A. Henderson-Sellers, P. J. Kennedy, and M. F. Wilson, 1986: Biosphere–atmosphere transfer scheme (BATS) for the NCAR Community Climate Model. NCAR Tech. Note NCAR/TN-275+STR, 69 pp., doi:10.5065/D6668B58.

Downing, T. E., and M. L. Parry, 1994: Introduction: Climate change and world food security. *Food Policy,* **19,** 99–104, doi:10.1016/0306-9192(94)90063-9.

Drexler, J. Z., R. L. Snyder, D. Spano, and K. T. Paw U, 2004: A review of models and micrometeorological methods used to estimate wetland evapotranspiration. *Hydrol. Processes,* **18,** 2071–2101, doi:10.1002/hyp.1462.

Ek, M. B., K. E. Mitchell, Y. Lin, E. Rogers, P. Grunmann, V. Koren, G. Gayno, and J. D. Tarpley, 2003: Implementation of Noah land-surface model advances in the NCEP operational mesoscale Eta model. *J. Geophys. Res.,* **108,** 8851, doi:10.1029/2002JD003296.

Fereres, E., and M. A. Soriano, 2006: Deficit irrigation for reducing agricultural water use. *J. Exp. Bot.,* **58,** 147–159, doi:10.1093/jxb/erl165.

Foken, T., 2008: The energy balance closure problem: An overview. *Ecol. Appl.,* **18,** 1351–1367, doi:10.1890/06-0922.1.

Gowda, P. H., J. L. Chàvez, P. D. Colaizzi, S. R. Evett, T. A. Howell, and J. A. Tolk, 2007: Remote sensing based energy balance algorithms for mapping ET: Current status and future challenges. *Trans. ASABE,* **50,** 1639–1644, doi:10.13031/2013.23964.

Hart, Q. J., M. Brugnach, B. Temesgen, C. Rueda, S. L. Ustin, and K. Frame, 2009: Daily reference evapotranspiration for California using satellite imagery and weather station measurement interpolation. *Civ. Eng. Environ. Syst.,* **26,** 19–33, doi:10.1080/10286600802003500.

Hayhoe, K. B., and Coauthors, 2004: Emissions pathways, climate change, and impacts on California. *Proc. Natl. Acad. Sci. USA,* **101,** 12 422–12 427, doi:10.1073/pnas.0404500101.

Hollinger, D. Y., and A. D. Richardson, 2005: Uncertainty in eddy covariance measurements and its application to physiological models. *Tree Physiol.,* **25,** 873–885, doi:10.1093/treephys/25.7.873.

Homer, C., and Coauthors, 2007: Completion of the 2001 National Land Cover Database for the conterminous United States. *Photogramm. Eng. Remote Sens.,* **73** (4), 337–341. [Available online at www.asprs.org/a/publications/pers/2007journal/april/highlight.pdf.]

Houghton, J. T., Y. Ding, D. J. Griggs, M. Noguer, P. J. van der Linden, X. Dai, K. Maskell, and C. A. Johnson, Eds., 2001: *Climate Change 2001: The Scientific Basis.* Cambridge University Press, 881 pp.

Jackson, R. D., R. J. Reginato, and S. B. Idso, 1977: Wheat canopy temperatures: A practical tool for evaluating water requirements. *Water Resour. Res.,* **13,** 651–656, doi:10.1029/WR013i003p00651.

——, M. S. Moran, L. W. Gay, and L. H. Raymond, 1987: Evaluating evaporation from field crops using airborne radiometry and ground-based meteorological data. *Irrig. Sci.,* **8,** 81–90, doi:10.1007/BF00259473.

Jiménez, C., and Coauthors, 2011: Global intercomparison of 12 land surface heat flux estimates. *J. Geophys. Res.,* **116,** D02102, doi:10.1029/2010JD014545.

Kalma, J., T. R. McVicar, and M. F. McCabe, 2008: Estimating land surface evaporation: A review of methods using remotely sensing surface temperature data. *Surv. Geophys.,* **29,** 421–469, doi:10.1007/s10712-008-9037-z.

Kiparsky, M., and P. H. Gleick, 2003: Climate change and California water resources: A survey and summary of the literature. Rep. 500-04073, Pacific Institute for Studies in Development, Environment, and Security, Oakland, CA, 46 pp. [Available online at http://www.pacinst.org/reports/climate_change_and_california_water_resources.pdf.]

Knowles, N., and D. R. Cayan, 2002: Potential effects of global warming on the Sacramento/San Joaquin watershed and the San Francisco estuary. *Geophys. Res. Lett.*, **29,** 1891, doi:10.1029/2001GL014339.

Koch, G. W., and H. A. Mooney, 1996: Response of terrestrial ecosystems to elevated CO_2: A synthesis and summary. *Carbon Dioxide and Terrestrial Ecosystems,* G. W. Koch and H. A. Mooney, Eds., Academic Press, 443 pp.

Körner, C., 2000: Biosphere responses to CO_2 enrichment. *Ecol. Appl.,* **10,** 1590–1619. [Available online at www.jstor.org/stable/2641226.]

Kunkel, K. E., and Coauthors, 2008: Observed changes in weather and climate extremes. Weather and climate extremes in a changing climate—Regions of focus: North America, Hawaii, Caribbean, and U.S. Pacific islands, T. R. Karl et al., Eds., Synthesis and Assessment Product 3.3, U.S. Climate Change Science Program and Subcommittee on Global Change Research, Washington, DC, 35–80. [Available online at www.agci.org/dB/PDFs/Publications/07S1_USCCSP.pdf.]

Lawrence, D., and Coauthors, 2011: Parameterization improvements and functional and structural advances in version 4 of the Community Land Model. *J. Adv. Model. Earth Syst.,* **3,** M03001, doi:10.1029/2011MS00045.

Livneh, B., Y. Xia, K. E. Mitchell, M. B. Ek, and D. P. Lettenmaier, 2010: Noah LSM snow model diagnostics and enhancements. *J. Hydrometeor.,* **11,** 721–738, doi:10.1175/2009JHM1174.1.

Mahrt, L., 2010: Computing turbulent fluxes near the surface: Needed improvements. *Agric. For. Meteor.,* **150,** 501–509, doi:10.1016/j.agrformet.2010.01.015.

Marras, S., R. D. Pyles, C. Sirca, K. T. Paw U, R. L. Snyder, P. Duce, and D. Spano, 2011: Evaluation of the Advanced

Canopy–Atmosphere–Soil Algorithm (ACASA) model performance over Mediterranean maquis ecosystem. *Agric. For. Meteor.,* **151,** 730–745, doi:10.1016/j.agrformet.2011.02.004.

McElrone, A. J., T. M. Shapland, A. Calderon, L. Fitzmaurice, K. T. Paw U, and R. L. Snyder, 2013: Surface renewal: An advanced micrometeorological method for measuring and processing field-scale energy flux density data. *J. Visualized Exp.,* **82,** e50666, doi:10.3791/50666.

Meyers, T. P., 1985: A simulation of the canopy microenvironment using higher order closure principles. Ph.D. dissertation, Purdue University, 153 pp.

——, and K. T. Paw U, 1986: Testing of a higher-order closure model for airflow within and above plant canopies. *Bound.-Layer Meteor.,* **37,** 297–311, doi:10.1007/BF00122991.

——, and ——, 1987: Modelling the plant canopy micrometeorology with higher order closure principles. *Agric. For. Meteor.,* **41,** 143–163, doi:10.1016/0168-1923(87)90075-X.

Mooney, H. A., and Coauthors, 1999: Ecosystem physiology responses to global change. *Implications of Global Change for Natural and Managed Ecosystems: A Synthesis of GCTE and Related Research,* IGBP Book Series, No. 4, Cambridge University Press, 141–189.

Mueller, B., and Coauthors, 2011: Evaluation of global observations-based evapotranspiration datasets and IPCC AR4 simulations. *Geophys. Res. Lett.,* **38,** L06402, doi:10.1029/2010GL046230.

NCEP, 2012: NCEP North American Regional Reanalysis (NARR) dataset ds608.0. National Center for Atmospheric Research, Boulder, CO, digital media. [Available online at http://rda.ucar.edu/datasets/ds608.0/.]

Norman, J., W. P. Kustas, and K. S. Humes, 1995: Source approach for estimating soil and vegetation energy fluxes from observations of directional radiometric surface temperature. *Agric. For. Meteor.,* **77,** 263–293, doi:10.1016/0168-1923(95)02265-Y.

Owensby, C. E., P. I. Coyne, J. M. Ham, L. M. Auen, and A. K. Knapp, 1993: Biomass production in a tallgrass prairie ecosystem exposed to ambient and elevated CO_2. *Ecol. Appl.,* **3,** 644–653, doi:10.2307/1942097.

Paw U, K. T., 1997: The modeling and analysis of crop canopy interactions with the atmosphere under global climatic change conditions. *J. Agric. Meteor.,* **52,** 419–428, doi:10.2480/agrmet.52.419.

——, and W. Gao, 1988: Applications of solutions to non-linear energy budget equations. *Agric. For. Meteor.,* **43,** 121–145, doi:10.1016/0168-1923(88)90087-1.

Pimentel, D., and Coauthors, 2004: Water resources: Agricultural and environmental issues. *BioScience,* **54,** 909–918, doi:10.1641/0006-3568(2004)054[0909:WRAAEI]2.0.CO;2.

Pyles, R. D., 2000: The development and testing of the UCD Advanced Canopy–Atmosphere–Soil Algorithm (ACASA) for use in climate prediction and field studies. Ph.D. dissertation, University of California, Davis, 194 pp.

——, B. C. Weare, and K. T. Paw U, 2000: The UCD Advanced-Canopy-Atmosphere-Soil Algorithm (ACASA): Comparisons with observations from different climate and vegetation regimes. *Quart. J. Roy. Meteor. Soc.,* **126,** 2951–2980, doi:10.1002/qj.49712656917.

——, ——, ——, and W. Gustafson, 2003: Coupling between the UCD Advanced-Canopy-Atmosphere-Soil Algorithm (ACASA) and MM5: Preliminary results for July 1998 for western North America. *J. Appl. Meteor.,* **42,** 557–569, doi:10.1175/1520-0450(2003)042<0557:CBTUOC>2.0.CO;2.

Raupach, M. R., and J. J. Finnigan, 1995: Scale issues in boundary-layer meteorology: Surface energy balances in heterogeneous terrain. *Hydrol. Processes,* **9,** 589–612, doi:10.1002/hyp.3360090509.

Sanden, B., 2007: Fall irrigation management in a drought year for almonds, pistachios and citrus. *Kern Soil and Water Newsletter,* September 2007, University of California Cooperative Extension, Bakersfield, CA, 1–8. [Available online at http://cekern.ucanr.edu/files/98822.pdf.]

Seguin, B., 1989: Use of surface temperature in agrometeorology. *Applications of Remote Sensing in Agrometeorology,* F. Toselli, Ed., Springer, 221–240, doi:10.1007/978-94-009-2235-8_9.

Sellers, P. J., Y. Mintz, Y. C. Sud, and A. Dalcher, 1986: A simple biosphere model (SIB) for use with general circulation models. *J. Atmos. Sci.,* **43,** 505–531, doi:10.1175/1520-0469(1986)043<0505:ASBMFU>2.0.CO;2.

Simard, M., N. Pinto, J. Fisher, and A. Baccini, 2011: Mapping forest canopy height globally with spaceborne lidar. *J. Geophys. Res.,* **116,** G04021, doi:10.1029/2011JG001708.

Skamarock, W. C., and Coauthors, 2008: A description of the Advanced Research WRF version 3. NCAR Tech. Note NCAR/TN-475+STR, 113 pp. [Available online at http://www.mmm.ucar.edu/wrf/users/docs/arw_v3.pdf.]

Snyder, R. L., D. Spano, P. Duce, K. T. Paw U, and M. Rivera, 2008: Surface renewal estimation of pasture evapotranspiration. *J. Irrig. Drain. Eng.,* **134,** 716–721, doi:10.1061/(ASCE)0733-9437(2008)134:6(716).

Staudt, K., E. Falge, R. D. Pyles, and T. Foken, 2010: Sensitivity and predictive uncertainty of the ACASA model at a spruce forest site. *Biogeosci. Discuss.,* **7,** 4223–4271, doi:10.5194/bgd-7-4223-2010.

Suleiman, A., and R. Crago, 2002: Analytical land–atmosphere radiometer model. *J. Appl. Meteor.,* **41,** 177–187, doi:10.1175/1520-0450(2002)041<0177:ALARM>2.0.CO;2.

Trezza, R., 2002: Evapotranspiration using a satellite-based surface energy balance with standardized ground control. Ph.D. dissertation, Utah State University, 317 pp.

USDA, 2010: California almond forecast. National Agricultural Statistics Service, Washington, DC, 2 pp. [Available online at www.nass.usda.gov/Statistics_by_State/California/Publications/Fruits_and_Nuts/201005almpd.pdf.]

——, 2011: Noncitrus fruits and nuts 2010 summary. National Agricultural Statistics Service Washington, DC, 82 pp. [Available online at http://usda01.library.cornell.edu/usda/nass/NoncFruiNu//2010s/2011/NoncFruiNu-07-07-2011.pdf.]

van der Tol, C., and G. N. Parodi, 2012: Guidelines for remote sensing of evapotranspiration. *Evapotranspiration—Remote Sensing and Modeling,* A. Irmak, Ed., InTech, 227–250, doi:10.5772/18582.

Vaux, J. V., 1999: Q & A: Devising a water strategy for the 21st century. *Calif. Agric.,* **53,** 8–10.

Vinukollu, R. K., R. Meynadier, J. Sheffield, and E. F. Wood, 2011: Multi-model, multi-sensor estimates of global evapotranspiration: Climatology, uncertainties and trends. *Hydrol. Processes,* **25,** 3993–4010, doi:10.1002/hyp.8393.

Xu, L., 2012: What do we learn from coupling a next generation land surface model to a mesoscale atmospheric model? Ph.D. thesis, University of California, Davis, 154 pp.

Yuan, H., Y. Dai, Z. Xiao, D. Ji, and W. Shangguan, 2011: Reprocessing the MODIS leaf area index products for land surface and climate modelling. *Remote Sens. Environ.,* **115,** 1171–1187, doi:10.1016/j.rse.2011.01.001.

Zarate-Valdez, J. L., M. L. Whiting, B. D. Lampinen, S. Metcalf, S. L. Ustin, and P. H. Brown, 2012: Prediction of leaf area index by vegetation indexes. *Comput. Electron. Agric.,* **85,** 24–32, doi:10.1016/j.compag.2012.03.009.